university of groningen

faculty of science and engineering

Radiative Association of Diatomic Molecules: HeH^+ in The Interstellar Medium

Kevin Pérez

university of groningen / faculty of science and engineering

University of Groningen

Radiative Association for Diatomic Molecules: HeH^+ in The Interstellar Medium

Master's Thesis

To fulfill the requirements for the degree of
Master of Chemistry
at University of Groningen under the supervision of
Prof. dr. Shirin Faraji (University of Groningen)
Prof. dr. Thomas La Cour Jansen (University of Groningen)
and
Prof. dr. Jerome Loreau (KU Leuven)

Kevin Pérez (S4930002)

July 26, 2023

Contents

Abstract

In the interstellar medium, the rovibrational population of molecular ions can be outside of local thermodynamic equilibrium conditions. In this case, it becomes relevant to describe the chemistry of these ions using state-to-state rate coefficients instead of thermal rate coefficients in astrochemical models. The goal of the project is to investigate the chemistry of HeH^+, a molecule present in planetary nebulae NGC 7027 and important for the early universe chemistry by calculating the missing data (radiative association) to implement it in a robust model.

In this work, the radiative association (RA) of the molecular ion HeH^+ is computed by using nonlocal thermodynamic equilibrium in the zero-density limit approach. To achieve this, firstly the potential energy curve (PEC) for each electronic state is calculated using the state average complete active space self-consistent field (SA-CASSCF) configuration interaction (CI) method. Subsequently, the eigenfunctions are calculated numerically and used to compute the partial and total cross sections. Finally, the state-to-state rate coefficients are obtained numerically.

The computed rate coefficients are in good agreement at higher temperatures with the results reported in the literature. However, there is a discrepancy in the intensity at lower temperatures and therefore, at lower energies. The possible explanation for this outcome is owing to the electronic potential used. The scattering processes are sensitive to the potential and the differences in the well depth of the curve suggested a variation in the behavior of the low-energy bound states and orbiting resonances. In addition, the state-to-state rate coefficients are calculated for the association of the molecule from the electronic state $A^1\Sigma^+$ to $X^1\Sigma^+$ and from the state $X^1\Sigma^+$ to $X^1\Sigma^+$. This information is relevant for new robust models to understand the chemistry of the HeH^+ in the interstellar medium better.

1 Introduction

Hydrogen and helium are the most abundant atoms in the universe. They participate in the most relevant processes such as the formation of stars, planets, galaxies, and the nucleosynthesis of different atoms. [1] Understanding these processes in detail could give insight into other mechanisms in the interstellar medium (ISM) and unravel new data about the early universe. Therefore, knowledge about their chemistry and the formation of new products is meaningful.

In this way, the cation HeH^+ was introduced under the sight of astronomers due to the suggestion of being the first molecule formed by the radiative association (RA) in the universe (Eq. 1) and its possible participation in the formation mechanisms of H_2 and H_2^+ (Eq. 2, 3)during the recombination era in the early universe. [2–4] These suggestions were supported with the rate coefficients calculated: [5–10]

$$He^+ + H \rightarrow HeH^+ + h\nu, \tag{1}$$

$$HeH^+ + H \rightarrow H_2^+ + He, \tag{2}$$

$$H_2^+ + H \rightarrow H_2 + H^+. \tag{3}$$

This idea set an exploration for finding this ion in the ISM. Firstly, In 1977, Dabrowski et al. reported the spectroscopy determination of the infrared rotation-vibration spectrum of the molecule and suggested its presence in the planetary nebulose NGC 7027. [11] Subsequently, during a few decades, many attempts to detect the molecule in dense clouds, specifically in the nebulose proposed by Dabrowski, were obstructed by the near frequency of the transition lines of CH. [12–15] Finally, in 2019 Güsten et al. made the first detection of the molecular ion through terahertz spectroscopy (GREAT) located in the high-altitude observatory (SOFIA) by observing the pure rotational transition $J = 1 \rightarrow 0$. [16] One year later, Neufeld et al. confirmed the presence of HeH^+ in NGC 7027 by detecting the emission transitions ν =1-0 for the branches P(1) and P(2). [17] This was possible by using the iSHELL spectrograph on NASA. However, they found a discrepancy between the strength of the lines detected and the models proposed in the past.

Besides the experimental results, considerable contributions have been made by the theoretical results. In this frame, data about the rate coefficients of the formation and destruction of HeH^+ have been reported. [18–20] On one hand, for the formation paths, the main mechanism considered is the radiative association. This mechanism studied the collision between two particles to form a stable molecule through the emission of a photon. On the other hand, for the destruction paths, collisions with molecular hydrogen and electron impacts are the principal routes treated. Furthermore, calculations of the reactivity of HeH^+ with other molecules have been studied by scattering processes and dynamical approaches. [21]

The theoretical studies are used to predict and model the cation in the different environments present in the ISM. [22] Currently, new models are being developed where the system is considered outside of thermal equilibrium. [23] In the case of HeH^+ this is appropriate, due to its higher reactivity owing to the ion nature and the conditions where it is believed the molecule is found. Therefore, this model allows studying the reactivity of the molecule at different excited ro-brivational states by including the state-to-state-resolved data from the formation and destruction mechanism, and the Einstein coef-

ficients. Nevertheless, the information regarding the formation is missing.

In this project, the data from state-to-state resolved for the formation path of HeH^+ through radiative association is calculated. This information is obtained by simulating the following reactions:

$$H^+ + He(1s^2) \rightarrow HeH^+(X^1\Sigma^+) + h\nu, \tag{4}$$

$$He^+(1s) + H(1s) \rightarrow HeH^+(X^1\Sigma^+) + h\nu, \tag{5}$$

$$He^+(1s) + H(1s) \rightarrow HeH^+(A^1\Sigma^+) + h\nu. \tag{6}$$

The correspondent cross sections and rate coefficients are calculated numerically. Similarly, the lifetimes of the transitions between vibrational levels are considered. Finally, the results obtained are useful for models that consider the non-local thermodynamical equilibrium.

2 Theoretical Methods

2.1 Potential Energy Curve

Scattering calculations, such as cross sections, are sensitive to the potential utilized. Thus, using accurate potentials is crucial to obtain reliable results. Here, to simulate the three different cases mentioned, three potentials are considered for the ground state ($X^1\Sigma^+$). The first one is taken from Pachucki. [24] He used asymptotically correct generalized Heitler-London functions with a large number of basis functions that made it possible to obtain an accuracy of 10^{-12} a.u. The second potential was calculated by Juřek et al. by using canonical SCF orbitals as molecular orbital basis in the CI approach. [8] Lastly, the Born-Oppenheimer potential energy curve for the ground ($X^1\Sigma^+$) and the excited state ($A^1\Sigma^+$) of HeH^+ were calculated as a function of the internuclear distance R using the Molpro software. [25] For both states the aug-cc-pV5Z (AV5Z) basis set was used for each atom. To perform the calculations, an SA-CASSCF using 19 orbitals in the active space followed by a configuration interaction (CI) was performed. [26, 27] The curves were obtained from a range from 0.7 to 2900 Bohr with different spaces between each point.

2.2 Eigenfunctions

The starting point for state-to-state calculations is the wavefunctions. In the case of a radiative association, the requirements are the vibrational bound states and the continuum wave functions. For both types of eigenfunctions, a different method is used, as described in the following.

2.2.1 Bound States

The robrivational states for each electronic curve are obtained by solving the nuclear time-independent Schrodinger equation (TISE) in the frame of the nuclear center of mass,

$$\left[-\frac{\hbar^2}{2\mu}\frac{d^2}{dR^2}+\frac{J(J+1)}{2\mu R^2}+V(R)-E_{\upsilon J}\right]\psi_{\upsilon J}(R)=0, \tag{7}$$

where $\mu = 1467.786$ is the reduced mass of the molecule, R is the internuclear distance, J is the angular quantum number, $V(R)$ is the PEC, and $E_{\upsilon J}$ are the eigenvalues of the robrivational states. This equation is solved numerically by using the discrete variable representation method (DVR) with a uniform grid (Appendix A). [28] In addition, to implement this approach, it is necessary to perform an interpolation of the potential. In this scenario, a cubic spline method is used. [29] Moreover, the eigenfunctions obtained are unity-normalized such as $\int \psi^2_{\upsilon J}(R)\, dR = 1$.

2.2.2 Continuum States

The spectrum of positive energies is continuous and goes from zero to infinity. Each eigenvalue is infinitely degenerate and thus, it is only required to obtain the wavefunction corresponding to each desired energy. To accomplish the above-mentioned, it is necessary to solve the TISE,

$$\left[\frac{d^2}{dr^2}+k^2-\frac{J(J+1)}{r^2}-V(R)\right]f_{kJ}=0 \tag{8}$$

where $k^2=\frac{2\mu E}{\hbar^2}$ is the wavenumber corresponding to the relative motion between the two atoms. To solve this differential equation a symplectic integrator described by Manolopoulos et al. is used. [30]

This approach is described in more detail in the appendices.

Subsequently, the continuum wave functions obtained are energy-normalized such that at $R \to \infty$ the wavefunction should behave as,

$$f_{kJ} \approx \left(\frac{2\mu}{\hbar^2 \pi k}\right)^{\frac{1}{2}} sin\left(kR - \frac{1}{2}J\pi + \eta_J\right) \tag{9}$$

with η_J describing the phase shift of the Jth partial wave. [31]

2.3 Cross Section

Under the radiative association process, and using the Fermi golden rule in the zero-density limit, the partial cross section is defined by the following equation,

$$\sigma(E,v,J) = \frac{64\pi^5 \nu^3 p}{3C^3 k^2}\left[JM^2_{v,J-1;k,J} + (J+1)M^2_{v,J+1;k,J},\right] \tag{10}$$

where ν is the emitted photon frequency, C is the speed of light, p is the initial factor in the initial electronic state, J is the initial rotational number, and $M_{v,J\pm1;k,J}$ is the electric dipole matrix elements expressed by,

$$M_{v,J\pm1;k,J} = \int_0^\infty \psi_{\upsilon,J\pm1}(R)\ \mu(R)\ f_{kJ}(R)\ dR. \tag{11}$$

These matrix elements are solved by numerical quadrature. The total cross section is reached considering the sum of the partial cross section over all the vibrational and rotational levels,

$$\sigma(E) = \sum_J \sum_v \sigma(E,V,J). \tag{12}$$

2.4 Rate Coefficient

With the total cross section introduced in the previous section, assuming Maxwellian velocity distribution of the initial states, and averaging over the normalized energy distribution the temperature-dependent rate coefficient is stated by:

$$\alpha(T) = \left(\frac{8}{\pi\mu}\right)^{\frac{1}{2}}\left(\frac{1}{k_b T}\right)^{\frac{3}{2}} \int_0^\infty E\sigma(E)e^{-E/k_b T}dE \tag{13}$$

where k_b is the Boltzmann constant and T is the temperature. [32] Similarly, this equation is solved using numerical quadrature.

2.5 Life time

Further analysis is done by studying the radiative lifetime of the vibrational states present in the studied electronic curves. This approach considered all the possible transitions between an initial excited vibrational state i to a lower state f. Thus, The inverse of the lifetime is expressed by the following equation: [33]

$$\tau^{-1} = \sum_f A_{if} = \frac{4}{3\hbar^4 c^3}\sum_f E^3_{if} < i|\mu|f >^2 \qquad only for E_i > E_f, \tag{14}$$

where A_{if} are the Einstein coefficients for spontaneous emission, E_{if} are the energy differences between the two vibrational states, and μ is the dipole moment.

3 Computational details

The steps to simulate the scattering process in this project are presented in Fig. 1. The first stage is the calculation of the vibrational functions and eigenenergies. For this, the Hamiltonian matrix is generated and diagonalized using the subroutine "DSYEV" from the LAPACK library. [34] Moreover, the convergence in energy is achieved by using a grid with 15000 points from 0 to 300 Bohr. This step is performed for all the rotational levels with bound states in each electronic curve.

The following step is to generate the grid in energies to compute the partial and total cross section. For all the reactions, the total cross section was calculated from 0.01 to 100000 cm^{-1}. In this case, an irregular grid was used, owing to the width of the peaks requiring a more detailed description in order to calculate the integrals in a solid way. Thus, an dE between 0.01 and 0.0001 cm^{-1} was utilized.

Using the grid previously generated, the continuum wave functions are calculated for each energy value using the symplectic propagator. This approach needs the boundary conditions and an initial guess. In this scheme, the condition that the wave function is zero at $R = 0$ is used as a boundary condition, and as an initial guess was assumed that the function is almost zero at short internuclear distances. In addition, the range of these functions was from 0 to 4000 Bohr with a $dR = 0.05$ Bohr.

Applying the wave functions obtained in the above steps, along with the dipole moments, the dipole matrix elements are computed by doing the integrals numerically. Multiplying by the factors in equation 10 the rotational and vibrational cross section is determined. Subsequently, doing the sum over all the levels, we calculated the total cross section as a function of the kinetic energy of the continuum states. Since each calculation in energy is independent, a parallelization is performed by using OpenMP. [35]

Lastly, the rate coefficients are calculated by integrating the previous results and following the Eq. 13. A temperature range from 1 to 20000 K is used with a $dT = 0.19$ K. Furthermore, It was verified that there were enough energy values to describe the distribution by solving Eq. 15 and obtaining values close to 1.

$$K(T) = \left(\frac{2}{\sqrt{\pi}}\right)\left(\frac{1}{k_b T}\right)^{\frac{3}{2}} \int_0^\infty \sqrt{E} e^{-E/k_b T} dE. \tag{15}$$

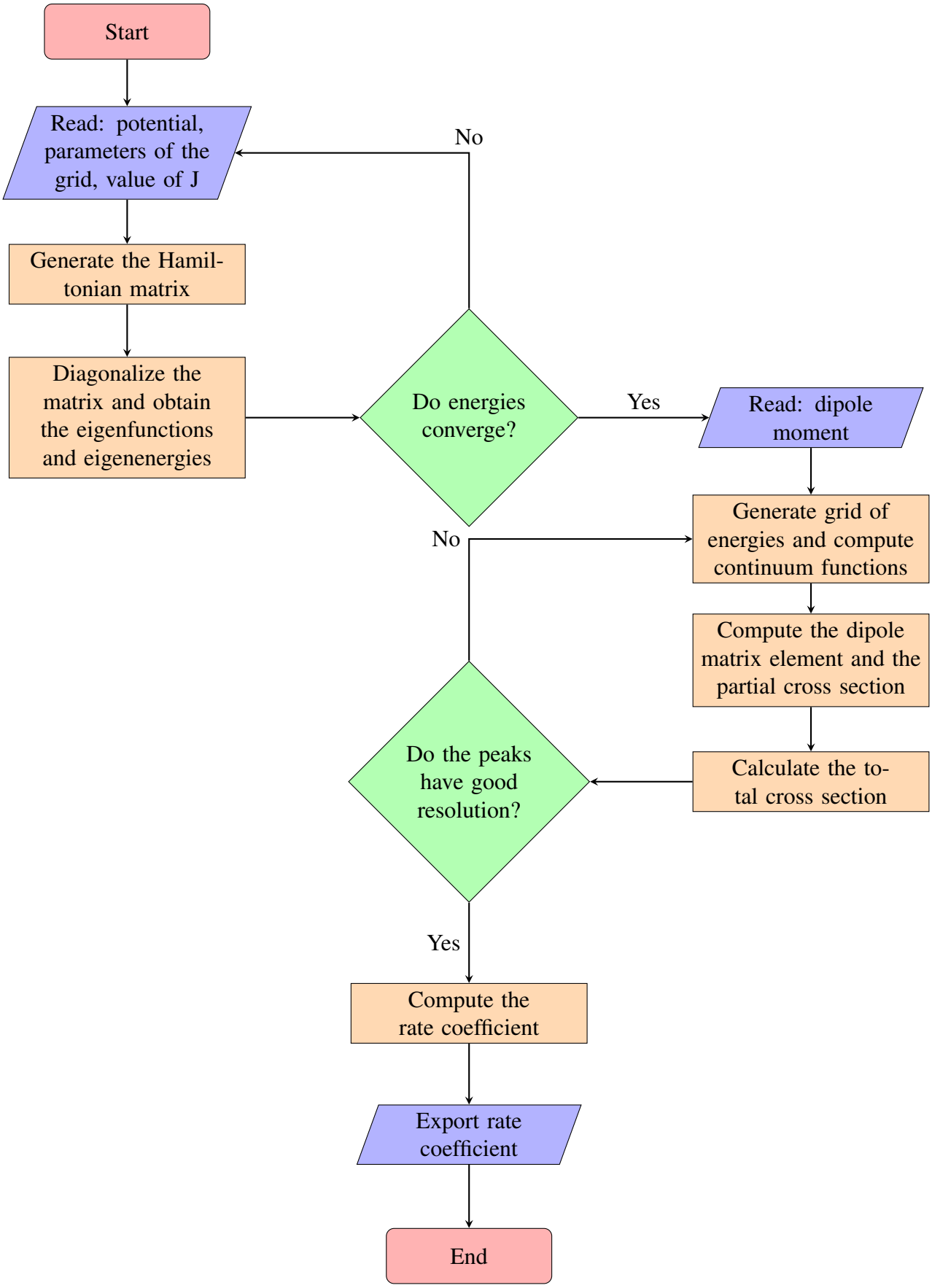

Figure 1: Flowchart of computational protocol followed in this project

4 Results and Discussion

4.1 Potential and Dipole Moment

Three PEC were used to calculate the eigenfunctions of the ground state of HeH^+. The accuracy of the potentials not only influences the energies and functions of the bound states, but also the continuum wave functions and the description of quasibound or orbiting resonances. Hence, one of the parameters linked with accuracy is the potential well depth. The differences in this parameter have an impact on the position and the behavior of the states with very low energy and are therefore crucial for the rate coefficient at low temperatures. A comparison of this parameter is presented in Table 1. As can be seen, the deviation between the results reported and the present work is appreciable. This variation in the potential well depth could potentially influence the eigenfunctions and eigenenergies.

Table 1: Comparison of the calculated potential well depth of the ground state ($X^1\Sigma^+$) of HeH^+ with results reported in the literature

Author	**Potential well depth(cm^{-1})**
1965 Wolniewicz [36]	16448.35057
1976 Kołos and Peek [37]	16455.9795
1979 Bishop and Cheung [38]	16448.3791
1994 Juřek et al. [8]	16443.87328
2012 Pachucki [24]	16457.07111
Present Work	16465.13514
Standard Deviation	7.731

The graph of the potentials is presented in Fig. 2. The first remarkable feature is the potential well depth, where the ground state poses a more extensive well than the excited state. This characteristic is reflected in the number of vibrational states present in each potential, obtaining 162 for the ground state and 32 for the excited state. In addition, there is a difference in the geometries between the curves, where the local minimum is located at different distances. This can be translated as a bad overlap between the vibrational levels of the two curves. This will be discussed in more detail in section 4.4.

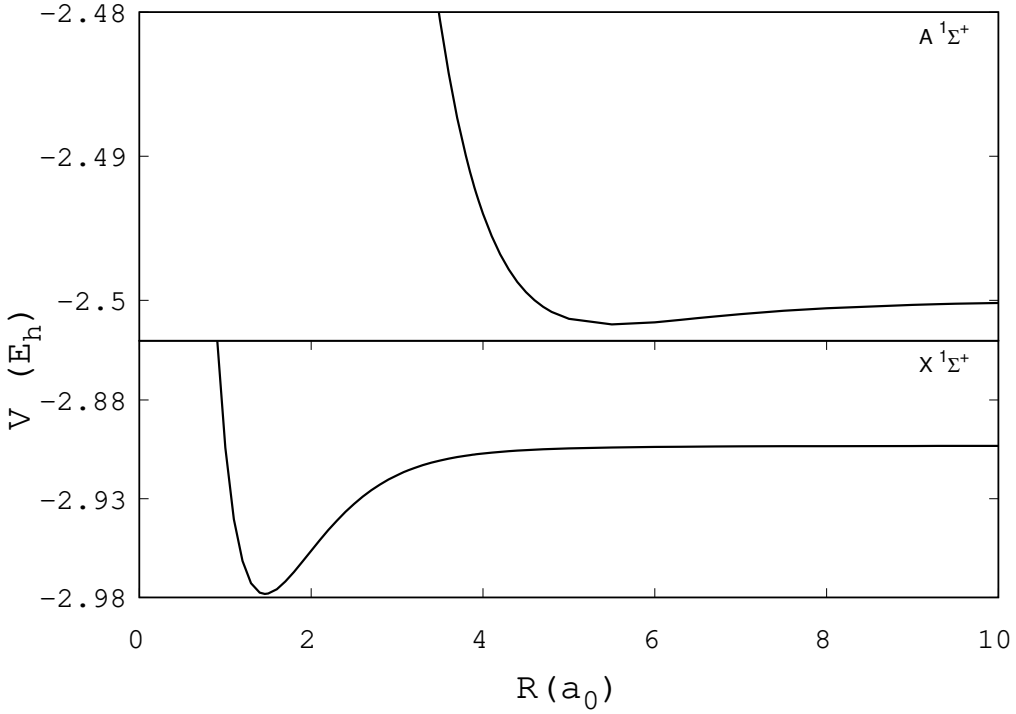

Figure 2: Adiabatic potential curves of the ground($X^1\Sigma^+$) and excited($A^1\Sigma^+$) state of HeH^+

Fig. 3 presents the permanent dipole moment of the ground and excited states, as well as the transition dipole moment between the two electronic states. The permanent dipole moments increase proportionally to the internuclear distance. This behavior agreed with the reported in the literature. [39] Conversely, the transition dipole moment has a maximum at short internuclear distances and decreases for longer distances. Similarly, it is found in good agreement with the reports in the literature. [5]

4.2 Eigenfunctions

In total, 23 rotational levels with bound vibrational states were found in the three electronic ground potentials. For the electronic excited state, only 11 rotational levels were calculated. The behavior of some of the vibrational levels ($\nu = 0,2,7,9$) obtained with the DVR for the rotational level $J = 2$ of the ground state is shown in figure 4. These levels have a well-known form similar to the wavefunctions for an anharmonic oscillator, where the quantum number ν indicates the number of nodes of the function. The energies of these wavefunctions are additionally obtained from the DVR. The values are compared with the previous results, finding a good agreement. [38,40] In Table 2 are listed the energy differences between the levels ν and $\nu+1$ for each electronic ground potential used in the rotational level $J = 0$, along with the values reported by Stanke et al., including relativistic corrections. [41] As observed, the values fluctuate for a few cm^{-1}, and even for the highest vibrational levels at lower energies, the differences are minimal. This result represents a good convergence in energy from the values obtained with the methodology applied.

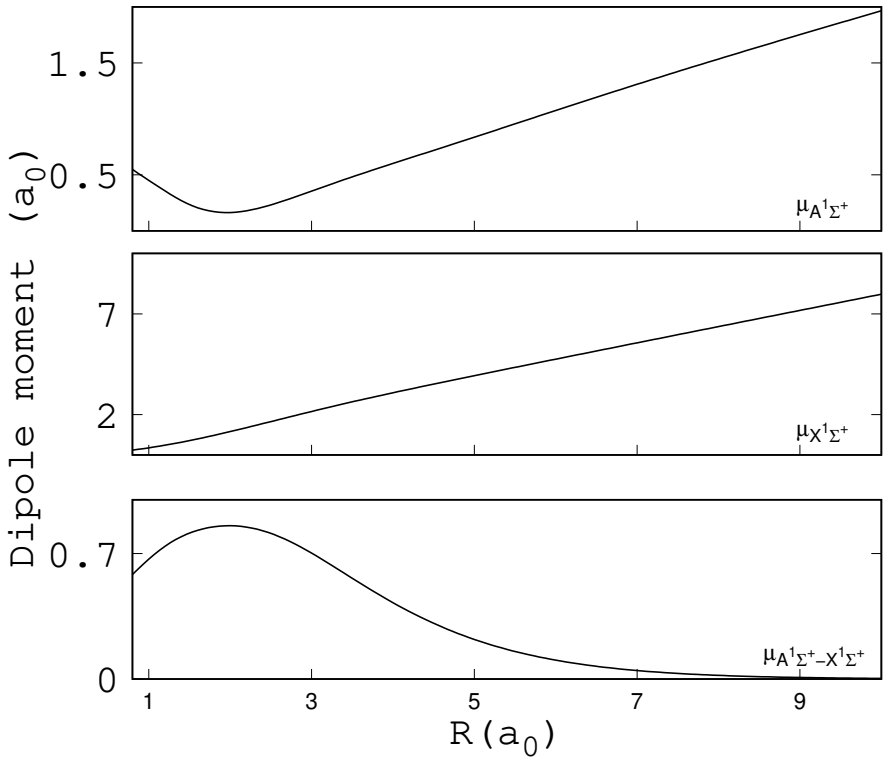

Figure 3: Permanent and transition dipole moment of HeH^+

Table 2: Comparison of vibrational frequencies ($\nu \rightarrow \nu + 1$) obtained using different electronic potential curve.

ν	ΔE^a(cm^{-1})	ΔE^b(cm^{-1})	ΔE^c(cm^{-1})	ΔE^d(cm^{-1})
0	2911.287	2909.139	2911.278	2911.000
1	2604.563	2601.602	2604.806	2604.167
2	2296.099	2296.212	2296.609	2295.578
3	1982.735	1980.671	1983.448	1982.056
4	1661.223	1660.360	1662.183	1660.355
5	1328.890	1327.667	1330.136	1327.786
6	985.692	985.045	987.214	984.359
7	640.657	639.824	642.356	639.195
8	328.634	332.373	329.984	327.361
9	116.846	115.289	117.063	116.148
10	24.655	23.838	24.752	24.409

[a] Obtained using the potential from the reference [24]
[b] Obtained using the potential from the reference [8]
[c] Present work
[d] Reported in Ref [41]

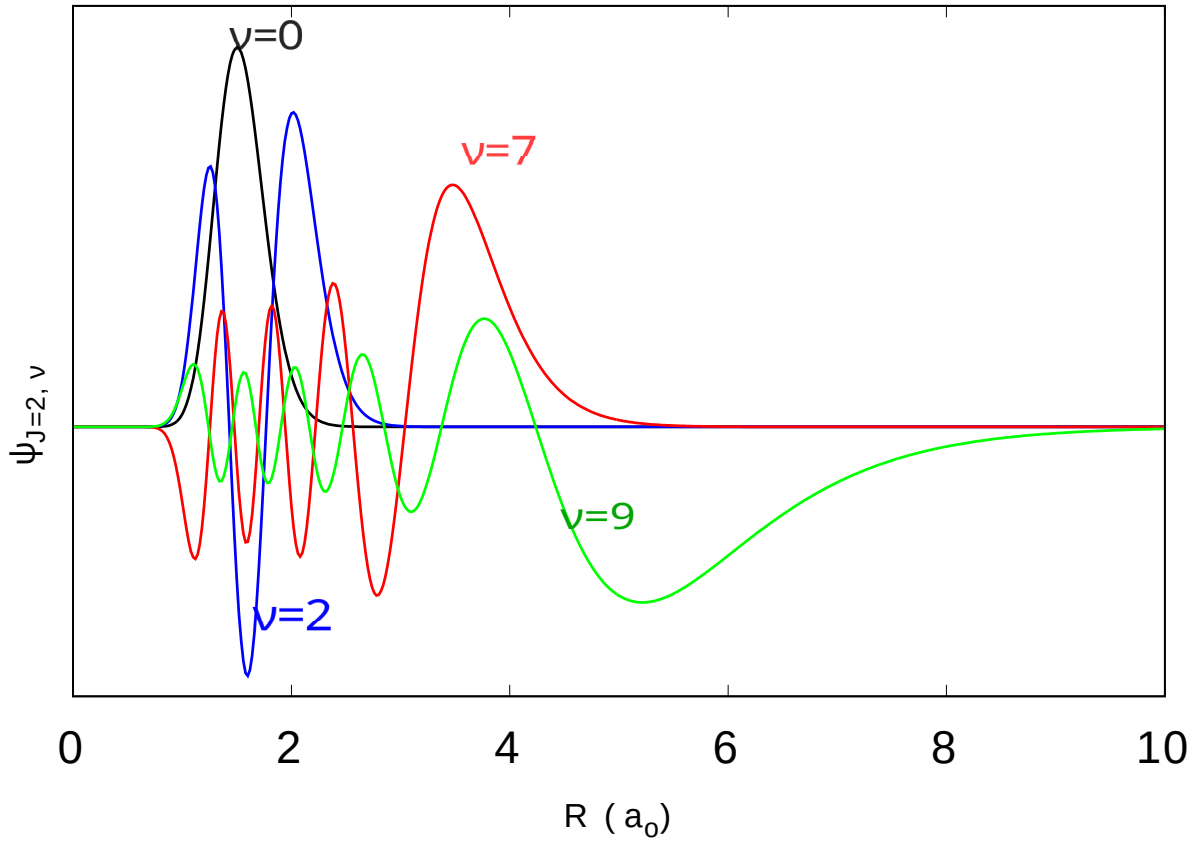

Figure 4: Vibrational wave functions $\psi_{J=2,\nu}$ of the cation HeH^+, where $\nu = 0,2,7,9$

Additional to the bound states, the continuum wave functions were obtained using a symplectic propagator. These propagators are numerical methods to solve the Hamiltonian evolutionary equations. For this case in particular, the evolution coordinate is not time, but is the radial coordinate. [30] Therefore, it is only necessary to know the boundary conditions, an initial guess, and the potential $V(R)$ to start to propagate the wavefunction.

The results obtained are presented in Fig. 5. The panel (a) shows the behavior of the eigenstate at low energies. Note how at short distances, there are no appreciable oscillations in the wave function. Instead, they start to be dominant at very long distances (around 2600 a_0). Furthermore, knowing the amplitude of these oscillations is essential to normalize the function (Eq. 9). To achieve this, it is required to have the information on the potential at longer distances because the methodology used requires these values to compute the eigenfunction at such long ranges. This singular behavior was the main limitation to use the different curves to calculate the continuum states, due to the reported electronic potentials lack of information at long ranges. Hence, all the continuum wave functions were only computed using the potentials calculated in this project. The panel (b) shows a continuum wave function at higher energies. In this case, there are some slow oscillations at short ranges and they become stronger proportional to the radial coordinate. Lastly, the plot in panel (c) displays the behavior of an orbiting resonance. These quasibound states are caused by the existence of the centrifugal potential and the quantum tunneling. [42] Its principal characteristics are the strong oscillation in the inner region of the potential and slow oscillation outside of it, completely opposite to the occurred at low and high energies. These features are similar to the bound states, and for this reason, this kind of wave function plays an important role in scattering processes.

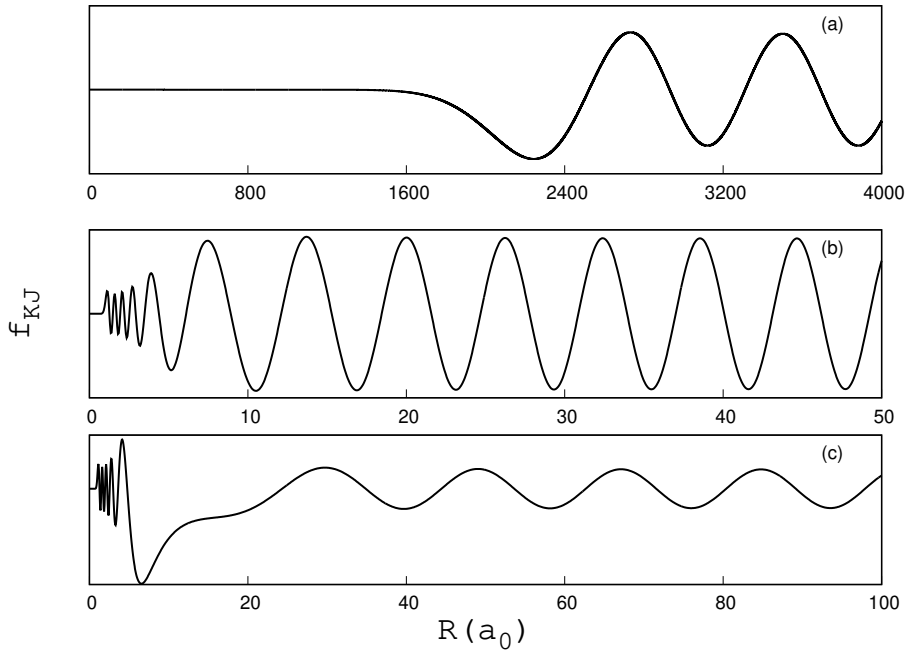

Figure 5: Behavior of the continuum wavefunctions at a) low energies b) High energies, and c) Quasi-bound /orbiting resonance.

In scattering studies, the cross section is a measurement of the frequency of collision per unit scatterer, relative to the flux of incident particles with respect to the target. [43] At the same time, this parameter can be related to transition probabilities as presented in Eq. 10. Thus, in this work, the partial and total cross sections of the formation of HeH^+ through radiative association were computed using the eigenfunctions, discussed in the previous section, and the different dipole moments mentioned in the section 4.1. For the reactions in Eq. 4 and 5, three different curves were used to obtain the set of bound states, therefore, three sets of results are presented. For the reaction in Eq. 6 only the excited electronic state is necessary, hence, the potential considered to calculate all the eigenfunctions was the one calculated in this project.

4.3 RA of the reaction $He(1s^2) + H^+ \rightarrow HeH^+ (X^1\Sigma^+)$

The first reaction studied was the RA, considering the molecule dissociated in the ground state as the initial state and the ion bounded in the electronic ground state as the final state(Fig 6). Fig. 7 shows the cross sections of this reaction (Eq. 4) as a function of the kinetic energy of the continuum wave functions. The plot presents the results using the three different potentials. Panel (a) shows the results obtained with the potential calculated. Panel (b) is obtained using the curve reported by Pachucki. Panel (c) displays the results obtained using the potential reported by Juřek et al. The three sets of results show a notable similarity between them, as the location and intensity of the peaks are indistinguishable. The main reason for this outcome is the fact that for all the cross sections, the same continuous wave functions were used. Consequently, the differences between using these curves remain in the bound states only, and, as presented in the Table 2, there are no big differences between the vibrational levels computed.

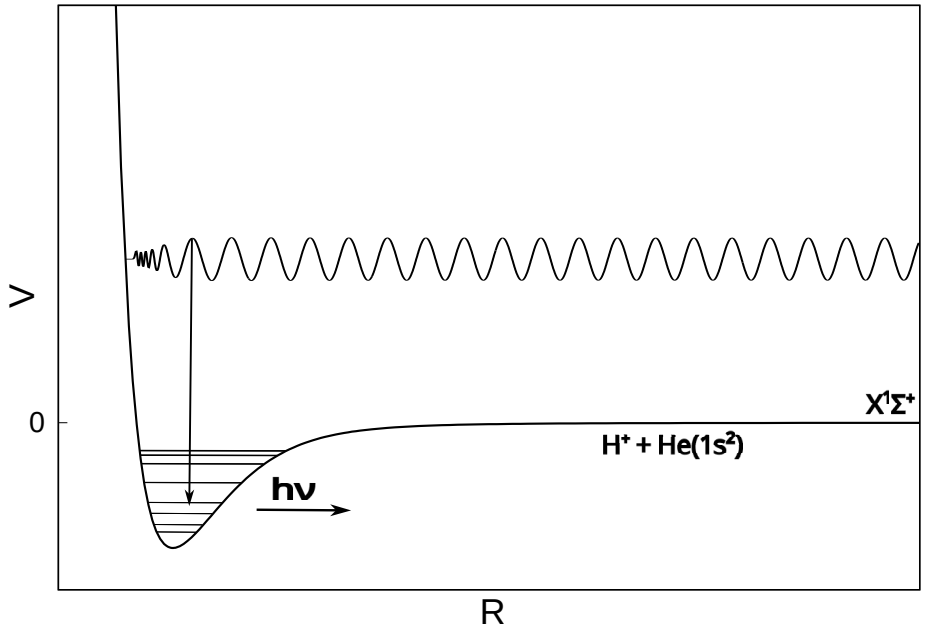

Figure 6: Sketch of the RA associated of the reaction $He(1S^2) + H^+ \rightarrow HeH^+$ $(X^1\Sigma^+)$. As the initial point, the continuum wave functions of the ground electronic state are used and these are tuned to the vibrational levels in the ground electronic state.

The existence of the strong and narrow peaks is the product of the substantial overlap between the resonances and the vibrational functions. As was mentioned in the previous section, these quasibound functions have similar behavior as any bound state. Consequently, the dipole matrix element, taking into account these functions, is going to be bigger than the one with the other kind of continuum wave functions presented in figure 5.

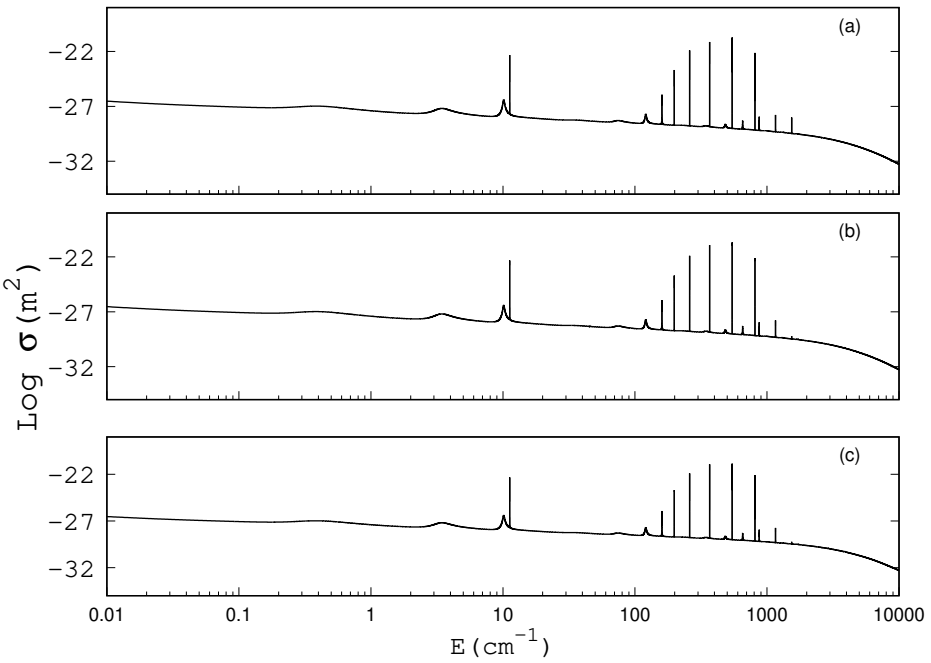

Figure 7: Total cross section of reaction $He(1s^2) + H^+ \rightarrow HeH^+$ $(X^1\Sigma^+)$ using a) calculated potential b) using Pachucki potential [24] c) using Juřek et al. potential [8]

Moreover, using the rotational and vibrational partial cross section, it is possible to find which rotational level contributes considerably to each peak, and, likewise, which vibrational level contributes substantially to the total cross section. Directly, with this analysis, it is possible to identify the rotational level and the energy at which the resonance is present. As an example, Fig. 8 shows on the panel (a), the partial rotational cross section of the level $J = 6$. The plot presents a strong peak located around 10 cm^{-1}. At the same energy in the plot of the total cross section (Fig. 7), is observed an identical strong peak with the same intensity. This indicates that this narrow peak is obtained by the main contribution of the orbiting resonance of the rotational level $J = 6$ at 10 cm^{-1}. Panel (b) of the graph plots the vibrational partial cross sections of the rotational level $J = 7$. In this case, the quasi-bound on $J = 6$ interacts with the vibrational levels of $J = 5$ and $J = 7$ due to the selection rules (Eq. 10). As is observed in the graph, all the vibrational levels contribute positively to the peak. However, the biggest overlap is achieved with the vibrational level $\nu = 5$. Similar behavior is obtained for the vibrational functions on $J = 5$, although their intensity is lower.

Applying the previous analysis, all the resonances were identified and compared with the reported in the literature, having a good agreement with them. [8, 37, 40, 44] In addition, the total cross section obtained in this work exhibits graphically vast similitudes with the one reported by Kraemer et al. and Juřek et al. [5, 8]

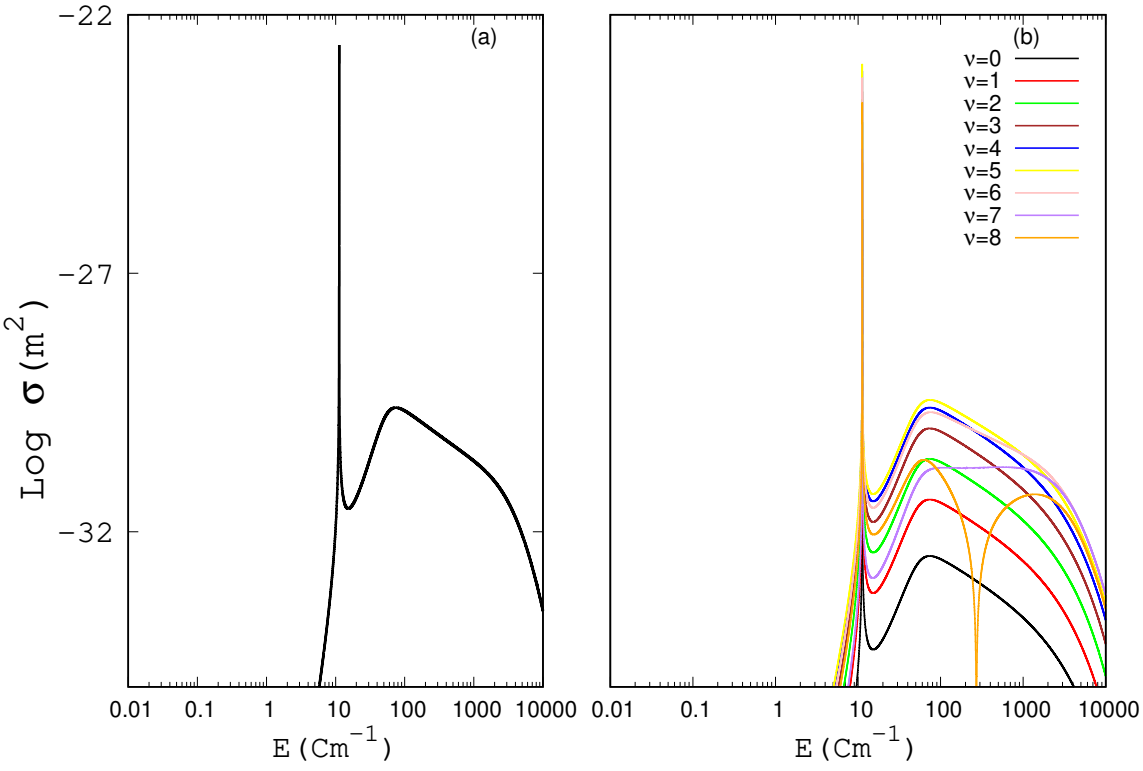

Figure 8: partial cross section a) for the rotational level $J = 6$ b) for all the vibrational levels present in $J = 7$

Using the total cross section and applying the Eq. 13, the rate coefficient is presented in Fig. 9, as a function of the temperature of the RA from the continuum wave function of the ground state to the robrivational functions of the same electronic state (Eq. 4). The results obtained using the three different potentials (Table 3-Appendix C) are compared with the results reported by Juřek et al., and

Zygelman et al. [8, 10] As can be observed, the highest intensity is reached around 10 K followed by a decrease, proportional to the increase in the temperature. This behavior occurs identically in the results reported. Nevertheless, the intensities for temperatures below 80 K are slightly different, whereas, at higher temperatures, there is an agreement. Moreover, the results reported by Zygelman et al. are different from each other because they used different potentials for their calculations. In addition, the three sets of results obtained in this project are almost equivalent to each other. This result could be predicted from the similarities presented in the results of the cross section (Fig. 7). This is a consequence of using the same PEC to obtain the continuum wave functions leading to similar cross sections and consequently, indistinguishable rate coefficients.

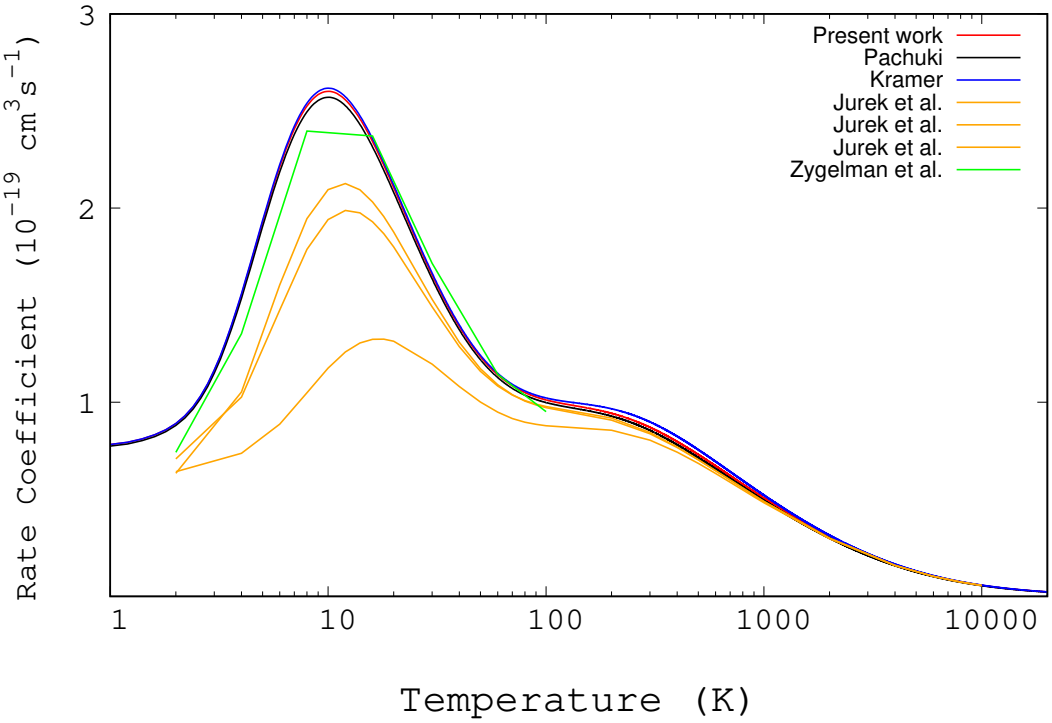

Figure 9: Rate coefficient of reaction 4

Similarly to the cross section, the results of the lifetime are proportional to the dipole matrix elements. However, for the lifetime, the states involved are entirely vibrational wave functions. Fig. 10 plots the lifetime as a function of the rotational and vibrational levels present in the reaction $He(1S^2) + H^+ \rightarrow HeH^+$ $(X^1\Sigma^+)$. The results indicate the highest intensity at $J = 1, \nu = 0$. This is a consequence of the big overlap between the vibrational wave function on $J = 1, \nu = 0$ and $J = 0, \nu = 0$. Additionally, according to Eq. 14, all the contributions between the initial state and the vibrational levels with less energy must be considered. In the case of $J = 1, \nu = 0$, the only state with less energy is $J = 1, \nu = 0$. Therefore, its lifetime is obtained by a single contribution inducing the high intensity. As the value of J is increasing, the intensity for the vibrational function with $\nu = 0$ decreases. This occurred as a result of considering more states which can give negative contributions to the total result in the calculation. The same behavior arises for the vibrational levels $\nu > 0$, where the positive and negative contributions cancel each other, given lower lifetimes.

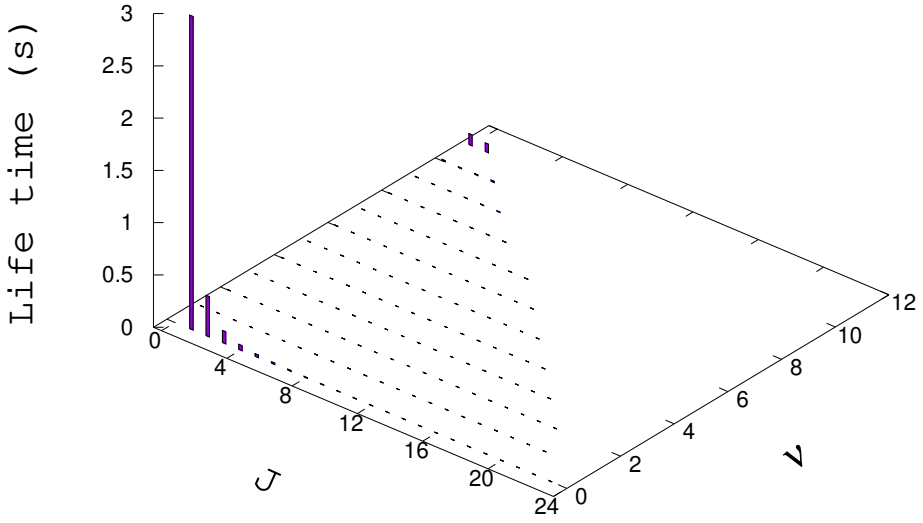

Figure 10: lifetime of the vibrational levels involved in reaction He($1s^2$) + H^+ → HeH^+ ($X^1\Sigma^+$)

4.4 RA of the reaction $He^+(1s^1)$ + $H(1s^1)$ → HeH^+ ($X^1\Sigma^+$)

In the second reaction (Eq. 5) studied, the starting point is the continuum wavefunctions on the excited electronic state $A^1\Sigma^+$ and the target is the vibrational levels on the ground electronic state $X^1\Sigma^+$. Fig. 11 shows the process. The first aspect to highlight is the big increase in the transition energy due to the addition of the energy difference between the ionization potentials of helium and hydrogen (0.4037 E_H). This modification induces a more extensive cross-section, and therefore, a bigger rate coefficient because the photon energy appears as ν^3 in the Eq. 10.

Fig. 12 displays the total cross section for reaction in Eq. 5. Similarly to the cross section presented in Fig. 7, the results obtained with each potential are almost identical to each other and have good agreement with the results reported by Kraemer et al. [5] However, the main difference between the total cross section presented in Fig. 7 and Fig. 12 is the presence of peaks. This is a consequence of the poor overlap between the resonances of $A^+\Sigma^+$ and the rovibrational functions of $X^+\Sigma^+$. As mentioned in the section 4.1, the differences between the potentials of the two electronic states could translate into a deficient overlap between the wavefunctions. Moreover, this result suggested that only low-energy quasibound are presented in the $A^+\Sigma^+$, since the peaks are observed only around 100 cm^{-1}.

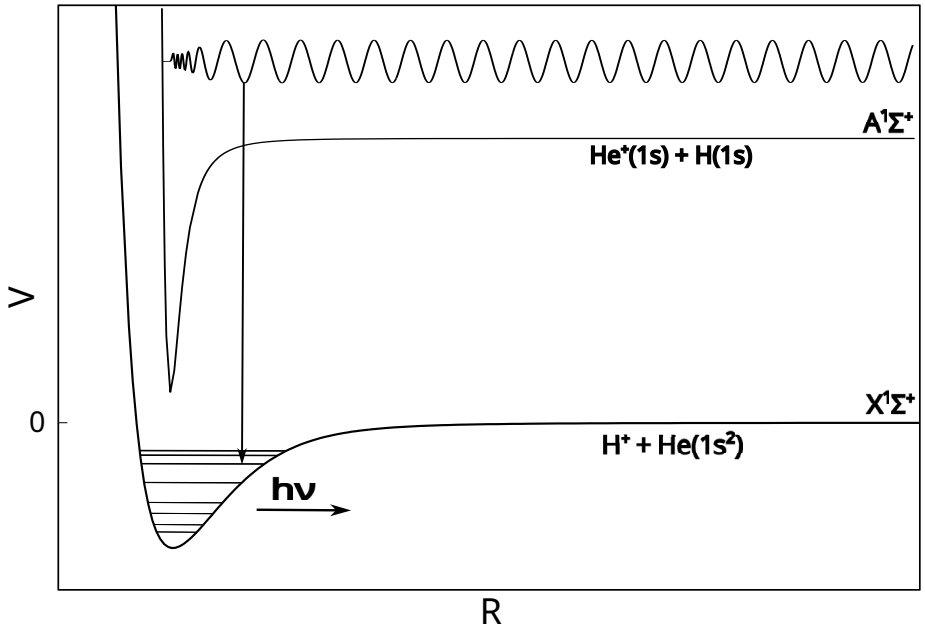

Figure 11: Sketch of the RA associated with the reaction $He^+(1s^1) + H(1s^1) \rightarrow HeH^+ (X^1\Sigma^+)$. The starting point is the continuum wave functions in the excited electronic state $A^1\Sigma^+$ which will interact with the robrivational functions of the ground electronic state $X^1\Sigma^+$

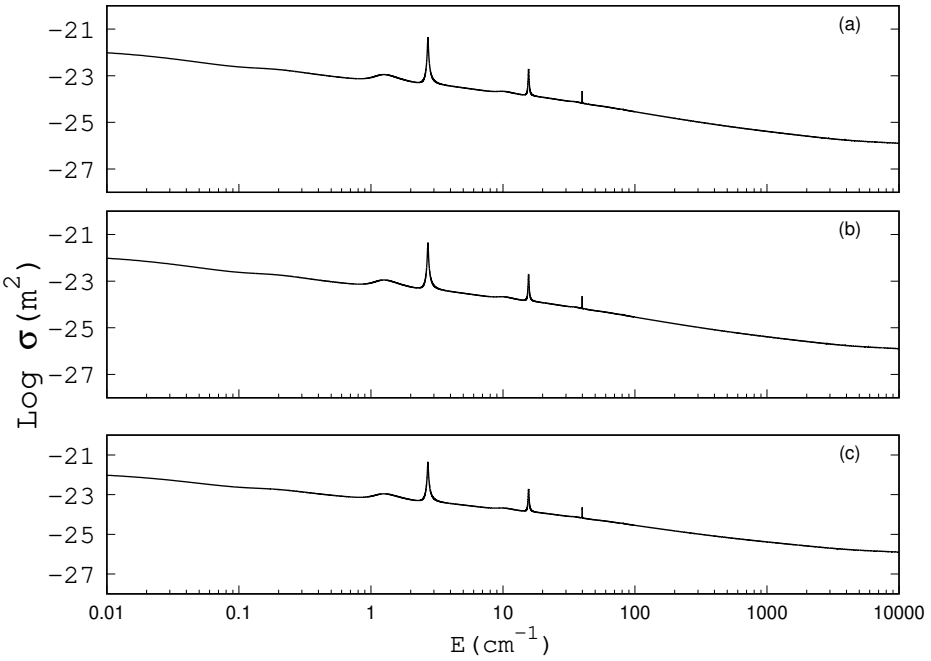

Figure 12: Total cross section of reaction $He^+(1s^1) + H(1s^1) \rightarrow HeH^+ (X^1\Sigma^+)$ a) this work b) using Pachucki potential [24] c) using Juřek et al. potential [8]

The rate coefficient of the RA of the reaction in Eq. 5 is presented in Fig. 13. The results (Table 4 - Appendix C) are compared with the values reported by Forrey et al., Kraemer et al., and Zygelman et al. [5, 6, 9] As can be seen, the values are 4 orders of magnitude bigger than for the reaction in section 4.3. This is the consequence of adding the energy factor to the photon frequency (Eq. 10),

as previously mentioned. In addition, the results computed differ from those reported at temperatures below 10 K, while similar behavior occurred in the rate coefficient of the reaction in section 4.3. There is, however, a good agreement at temperatures higher than 10 K until around two thousand kelvins. After this temperature, results from Kraemer et al. deviate from the rest. Furthermore, the three results computed in this project have a good correlation with each other. This outcome represents the consistency in the code programmed and its validity.

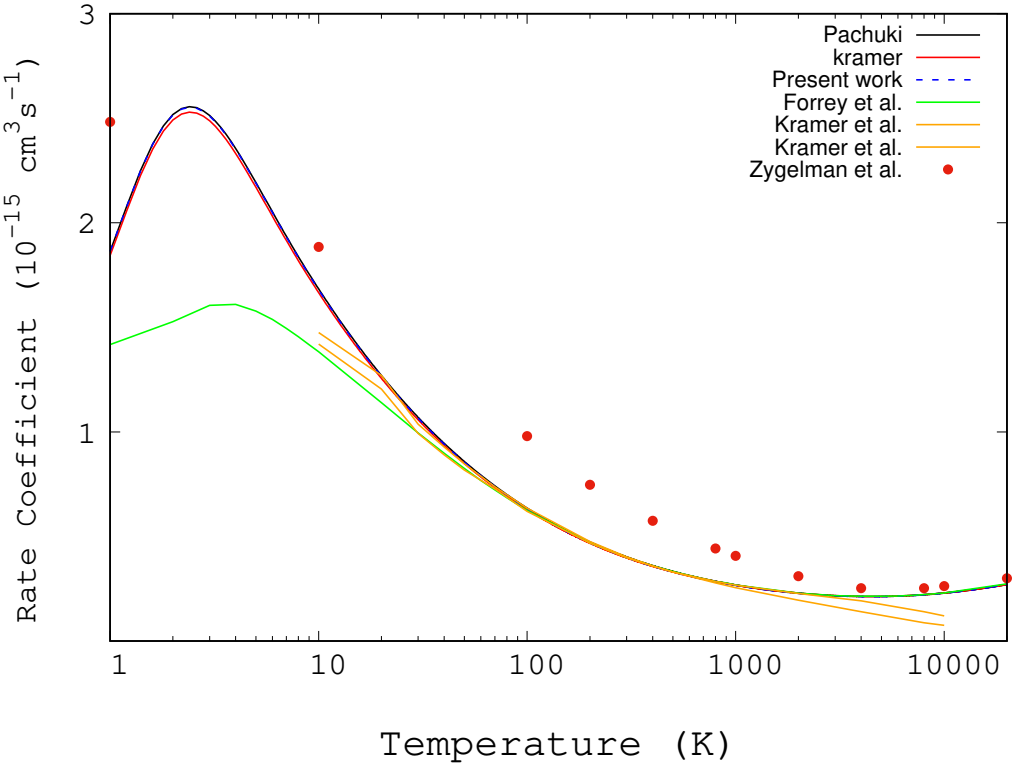

Figure 13: Rate coefficient as a function of the temperature of the reaction $He^+(1s^1)$ + $H(1s^1) \rightarrow HeH^+$ $(X^1\Sigma^+)$

Fig. 14 displays the lifetimes of the vibrational levels of the excited electronic state involved in the reaction $He^+(1s^1)$ + $H(1s^1) \rightarrow HeH^+$ $(X^1\Sigma^+)$. Contrary to the behavior observed in Fig. 10, the highest lifetimes are achieved with the highest vibrational levels ($\nu = 3,4$). In this situation, the initial states in the dipole matrix element (Eq. 14) are the vibrational levels of the excited electronic state, and the final states are vibrational wave functions of the ground electronic state. Since the eigenenergies from the ground state are lower than those from the excited state, all the wave functions from the ground state contribute to the lifetime of each vibrational level of the excited state. However, the values computed are six orders of magnitude smaller than in the anterior reaction. This is a consequence of the bad overlap between the vibrational levels of the excited electronic state and the wave functions of the ground electronic state.

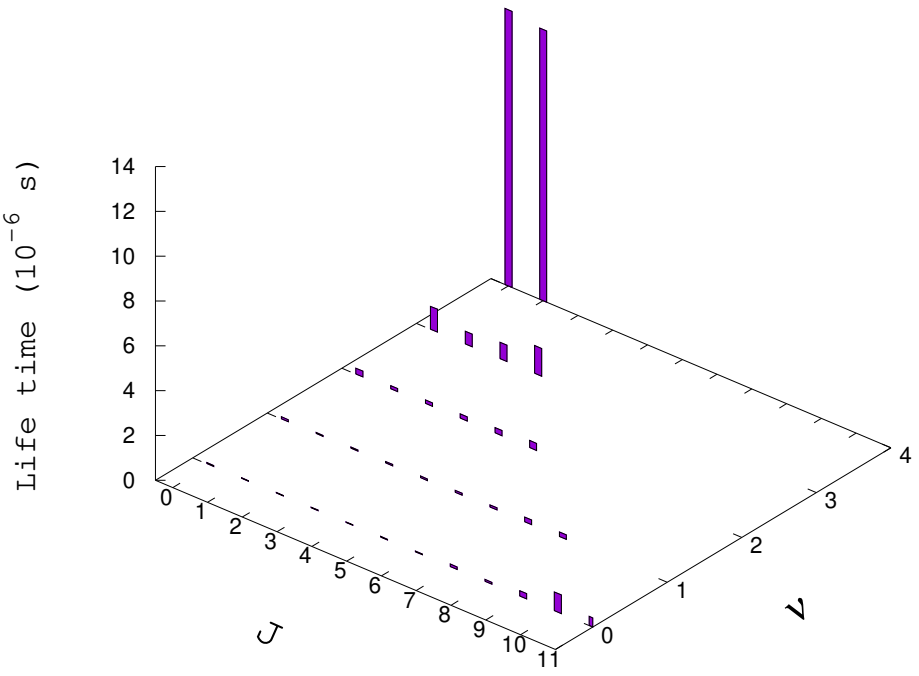

Figure 14: Lifetime of the vibrational levels involved in reaction $He^+(1s^1) + H(1s^1) \rightarrow HeH^+ (X^1\Sigma^+)$

4.5 RA of the reaction $He^+(1s^1)$ + $H(1s^1) \rightarrow HeH^+ (A^1\Sigma^+)$

The last reaction simulated (Eq. 6) takes place completely in the excited state $A^+\Sigma^+$. This process is sketched in Fig. 15. In this situation, the RA is achieved starting from the continuum to the bound states of the electronic excited state. Since the potential well depth of the excited state is smaller than the ground state, fewer contributions of the vibrational levels are expected. As mentioned in section 4.1, 32 vibrational levels belong to the electronic excited state, 130 less than the electronic ground state. This difference is reflected in the values of the total cross section and rate coefficient.

Fig. 16 shows the total cross section of the reaction in the Eq. 6. In this context, only the results obtained with the potential calculated are presented. Similar to the results of the total cross section for reaction in Eq.5, there are few peaks indicating the low presence of quasibound function on the potential. Certainly, the similitude of the positions of these peaks between Fig. 12 and Fig. 16 is notable. Thus, Fig. 17 shows this result in a more clear way, where panel (a) plots the partial rotational cross section of the reaction 5, whereas panel (b) plots the same result for the reaction 6. Both graphs demonstrate the existence of the resonances in the rotational levels $J = 3,5,6,8,9$,and 11. These states are responsible for the peaks in both cross sections because the same continuum wave functions were used.

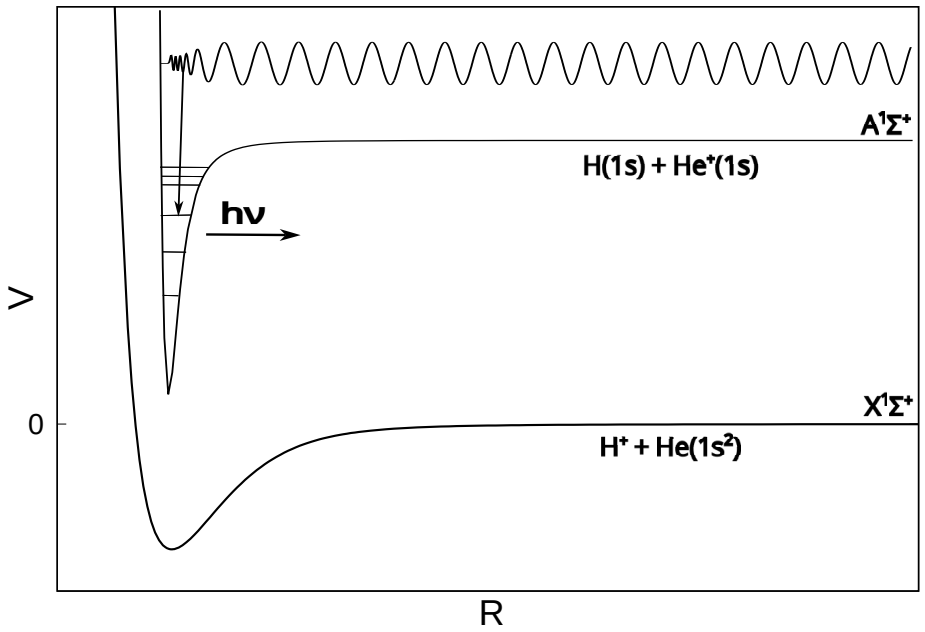

Figure 15: Sketch of the RA associated with the reaction $He^+(1s^1) + H(1s^1) \rightarrow HeH^+$ $(A^1\Sigma^+)$. The process occurred completely in the excited electronic state

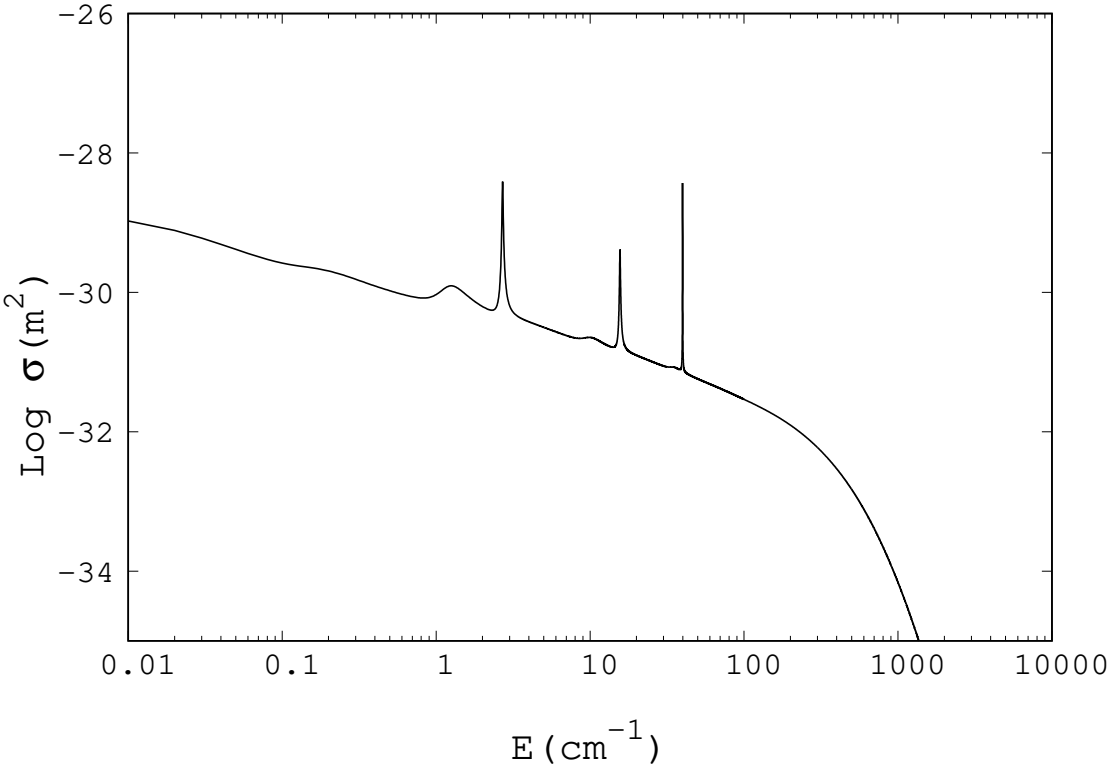

Figure 16: Total cross section of reaction $He^+(1s^1) + H(1s^1) \rightarrow HeH^+$ $(A^1\Sigma^+)$

The rate coefficient of this reaction is displayed in Fig. 18. The results, in the Table 5-Appendix C, show the highest values around 3 K. Above this temperature the rate coefficient decreases until the values are close to zero. This is a result of the low amount of orbiting resonances and the location

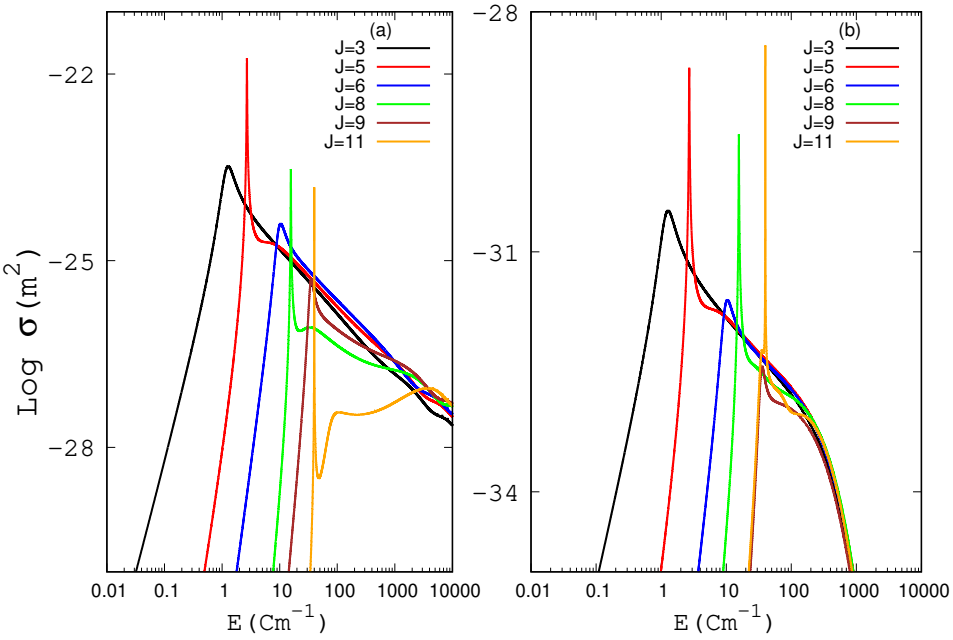

Figure 17: Partial rotational cross section a) Reaction $He^+(1s^1) + H(1s^1) \rightarrow HeH^+$ $(X^1\Sigma^+)$ b) Reaction $He^+(1s^1) + H(1s^1) \rightarrow HeH^+$ $(A^1\Sigma^+)$

of the peaks in the total cross section (Fig. 16) are at low energies, therefore the higher intensities are found at lower temperatures. Currently, there are no values reported in the literature. However, Kraemer et al. performed the same calculation and their results agree with the obtained in this project. [5] Lastly, the values of the rate coefficient of this reaction (Eq. 6) are the lowest among the possible formation path studied in this project. This result suggests that the formation of HeH^+, through RA involving only states in the $A^1\Sigma^+$ potential, is not as favorable as the other reactions.

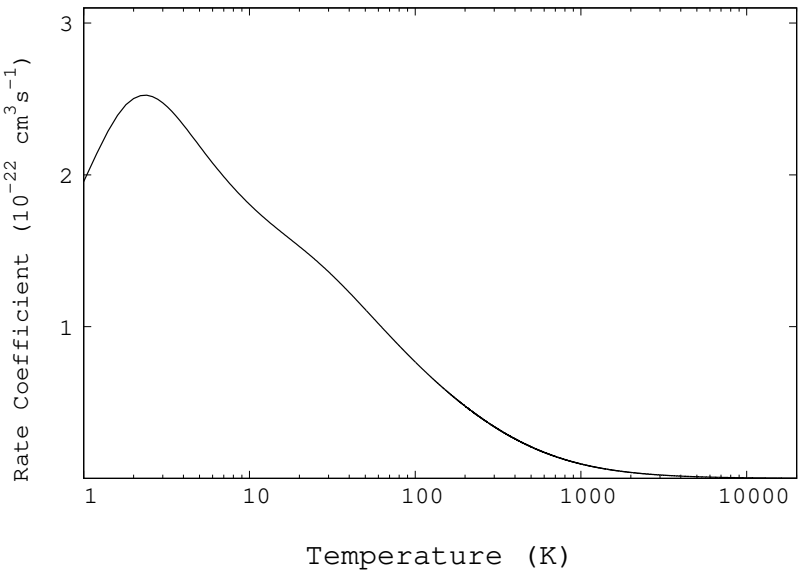

Figure 18: Rate coefficient as a function of the temperature of the reaction $He^+(1s^1) + H(1s^1) \rightarrow HeH^+$ $(A^1\Sigma^+)$

Finally, the lifetimes of the reaction (Eq. 6) are presented in Fig. 19. Since all the vibrational levels involved in this calculation are in the same electronic curve, the behavior obtained is similar to the one in Fig. 10. However, the values for this case are 100 times bigger. This is a result of the lower amount of vibrational functions since there are fewer states that could contribute negatively to the total sum (Eq. 14). In addition, the highest lifetime corresponds to wavefunction in $J = 1$, $\nu = 0$ due to its only contribution to the calculation is the pure rotational transition $J = 1, \nu = 0 \rightarrow J = 0, \nu = 0$.

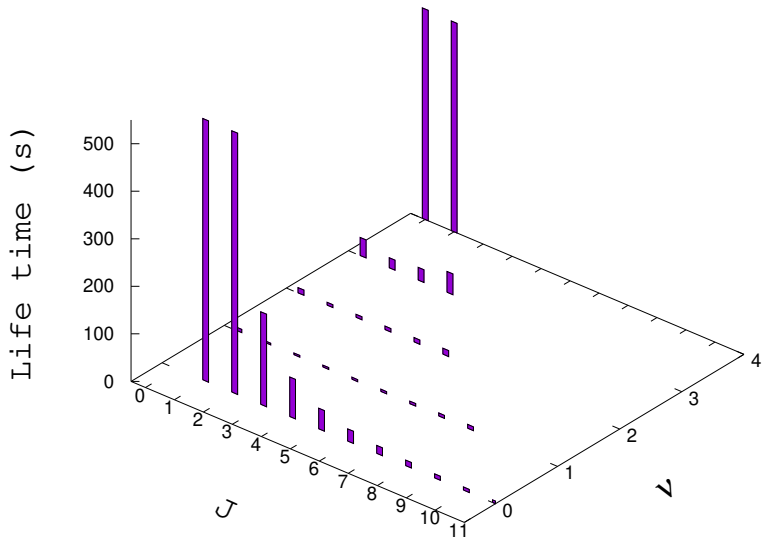

Figure 19: Lifetime of the reaction $He^{+}(1s^{1}) + H(1s^{1}) \rightarrow HeH^{+}$ $(A^{1}\Sigma^{+})$

5 Conclusion and Outlook

In conclusion, the partial and the total cross section, as well as the rate coefficient of the radiative association of HeH^+ were calculated under the nonlocal thermodynamic equilibrium in the zero-density limit. In addition, the lifetimes of the all vibrational levels present in the reactions 4, 5, 6 were computed by calculating the sum over the Einstein coefficients.

The consistency of the results of the cross sections and the rate coefficients between the electronic potentials used are a good proof of the validity of the code programmed. On the other hand, the difference in the intensity of the rate coefficient at lower temperatures, for the reactions 4 and 5, could be related to the fact that only the potentials calculated were used for the continuum wavefunctions. As a consequence, only the orbiting resonances belonging to these potentials interact with the vibrational levels of the other curves. Additionally, the differences in the potential well depth could represent deviations in the energies and shapes of the orbiting resonances, which have a direct impact on the cross section and therefore, on the rate coefficient.

Finally, the state-to-state rate coefficients were computed for reactions in Eq.4, 5. This information can be implemented in the new astrochemical model to describe the chemistry of HeH^+ in the ISM in a better way. Further work can be done on the new molecules discovered in the ISM related to this ion like HeH_3^+, CHe^{2+}, $HeHHe^+$, $HeHNe^+$, H_2He^+.

Bibliography

[1] A. M. Shaw, *Astrochemistry: From astronomy to astrobiology*. John Wiley & Sons, 2007.

[2] J. Black, "Molecules in planetary nebulae," *The Astrophysical Journal*, vol. 222, pp. 125–131, 1978.

[3] S. Lepp and J. M. Shull, "Molecules in the early universe," *Astrophysical Journal*, vol. 280, pp. 465–469, 1984.

[4] S. Lepp, P. Stancil, and A. Dalgarno, "Atomic and molecular processes in the early universe," *Journal of Physics B: Atomic, Molecular and Optical Physics*, vol. 35, no. 10, p. R57, 2002.

[5] W. Kraemer, V. Špirko, and M. Juřek, "Formation of heh+ by radiative association of he++ h. an advanced ab initio study," *Chemical physics letters*, vol. 236, no. 1-2, pp. 177–183, 1995.

[6] R. Forrey, J. Babb, E. Courtney, R. McArdle, and P. Stancil, "Revisiting the formation of heh+ in the planetary nebula ngc 7027," *The Astrophysical Journal*, vol. 898, no. 1, p. 86, 2020.

[7] E. Courtney, R. Forrey, R. McArdle, P. Stancil, and J. Babb, "Comprehensive chemistry of heh+ in the early universe," *The Astrophysical Journal*, vol. 919, no. 2, p. 70, 2021.

[8] M. Juřek, V. Špirko, and W. Kraemer, "Ab initio determination of the rate coefficient for radiative association of he (1s)+ h+," *Chemical physics*, vol. 193, no. 3, pp. 287–296, 1995.

[9] B. Zygelman and A. Dalgarno, "The radiative association of he (+) and h," *The Astrophysical Journal*, vol. 365, pp. 239–240, 1990.

[10] B. Zygelman, P. Stancil, and A. Dalgarno, "Stimulated radiative association of he and h+," *The Astrophysical Journal*, vol. 508, no. 1, p. 151, 1998.

[11] I. Dabrowski and G. Herzberg, "The predicted infrared spectrum of heh+ and its possible astrophysical importance," *Transactions of the New York Academy of Sciences*, vol. 38, pp. 14–25, 1977.

[12] X.-W. Liu, M. Barlow, A. Dalgarno, J. Tennyson, T. Lim, B. Swinyard, J. Cernicharo, P. Cox, J.-P. Baluteau, D. Pequignot, *et al.*, "An iso long wavelength spectrometer detection of ch in ngc 7027 and an heh+ upper limit," *Monthly Notices of the Royal Astronomical Society*, vol. 290, no. 4, pp. L71–L75, 1997.

[13] J. Moorhead, R. Lowe, J.-P. Maillard, W. Wehlau, and P. Bernath, "Search for heh (+) in ngc 7027," *The Astrophysical Journal*, vol. 326, pp. 899–904, 1988.

[14] H. L. Dinerstein and T. Geballe, "Detection and significance of [zn iv] 3.625 microns in planetary nebulae," *The Astrophysical Journal*, vol. 562, no. 1, p. 515, 2001.

[15] I. Zinchenko, V. Dubrovich, and C. Henkel, "A search for heh+ and ch in a high-redshift quasi-stellar object," *Monthly Notices of the Royal Astronomical Society: Letters*, vol. 415, no. 1, pp. L78–L80, 2011.

[16] R. Güsten, H. Wiesemeyer, D. Neufeld, K. M. Menten, U. U. Graf, K. Jacobs, B. Klein, O. Ricken, C. Risacher, and J. Stutzki, "Astrophysical detection of the helium hydride ion heh+," *Nature*, vol. 568, no. 7752, pp. 357–359, 2019.

[17] D. A. Neufeld, M. Goto, T. Geballe, R. Güsten, K. M. Menten, and H. Wiesemeyer, "Detection of vibrational emissions from the helium hydride ion (heh+) in the planetary nebula ngc 7027," *The Astrophysical Journal*, vol. 894, no. 1, p. 37, 2020.

[18] S. Miyake, C. Gay, and P. Stancil, "Rovibrationally resolved photodissociation of heh+," *The Astrophysical Journal*, vol. 735, no. 1, p. 21, 2011.

[19] M. Ayouz and V. Kokoouline, "Cross sections and rate coefficients for rovibrational excitation of heh+ isotopologues by electron impact," *Atoms*, vol. 7, no. 3, p. 67, 2019.

[20] C. Strömholm, J. Semaniak, S. Rosén, H. Danared, S. Datz, W. Van der Zande, and M. Larsson, "Dissociative recombination and dissociative excitation of heh+ 4: Absolute cross sections and mechanisms," *Physical Review A*, vol. 54, no. 4, p. 3086, 1996.

[21] F. Gianturco, K. Giri, L. Gonzalez-Sanchez, E. Yurtsever, N. Sathyamurthy, and R. Wester, "Energy-transfer quantum dynamics of heh+ with he atoms: Rotationally inelastic cross sections and rate coefficients," *The Journal of Chemical Physics*, vol. 154, no. 5, p. 054311, 2021.

[22] F. Van der Tak, J. H. Black, F. Schöier, D. Jansen, and E. F. van Dishoeck, "A computer program for fast non-lte analysis of interstellar line spectra-with diagnostic plots to interpret observed line intensity ratios," *Astronomy & Astrophysics*, vol. 468, no. 2, pp. 627–635, 2007.

[23] A. Faure, P. Halvick, T. Stoecklin, P. Honvault, M. Epée Epée, J. Z. Mezei, O. Motapon, I. Schneider, J. Tennyson, O. Roncero, *et al.*, "State-to-state chemistry and rotational excitation of ch+ in photon-dominated regions," *Monthly Notices of the Royal Astronomical Society*, vol. 469, no. 1, pp. 612–620, 2017.

[24] K. Pachucki, "Born-oppenheimer potential for heh+," *Physical Review A*, vol. 85, no. 4, p. 042511, 2012.

[25] H.-J. Werner, P. J. Knowles, G. Knizia, F. R. Manby, and M. Schütz, "Molpro: a general-purpose quantum chemistry program package," *WIREs Computational Molecular Science*, vol. 2, no. 2, pp. 242–253, 2012.

[26] H.-J. Werner and P. J. Knowles, "A second order multiconfiguration scf procedure with optimum convergence," *The Journal of chemical physics*, vol. 82, no. 11, pp. 5053–5063, 1985.

[27] P. J. Knowles and H.-J. Werner, "An efficient second-order mc scf method for long configuration expansions," *Chemical physics letters*, vol. 115, no. 3, pp. 259–267, 1985.

[28] D. T. Colbert and W. H. Miller, "A novel discrete variable representation for quantum mechanical reactive scattering via the s-matrix kohn method," *The Journal of chemical physics*, vol. 96, no. 3, pp. 1982–1991, 1992.

[29] W. H. Press, S. A. Teukolsky, W. T. Vetterling, and B. P. Flannery, *Numerical recipes in Fortran 90 the art of parallel scientific computing*. Cambridge university press, 1996.

[30] D. E. Manolopoulos and S. K. Gray, "Symplectic integrators for the multichannel schrödinger equation," *The Journal of chemical physics*, vol. 102, no. 23, pp. 9214–9227, 1995.

[31] L. D. Landau and E. M. Lifshitz, *Quantum mechanics: non-relativistic theory*, vol. 3. Elsevier, 2013.

[32] W. H. Smith, L. S. Liszt, and B. L. Lutz, "A reevaluation of the diatomic processes leading to ch and ch+ formation in the interstellar medium," *The Astrophysical Journal*, vol. 183, pp. 69–80, 1973.

[33] J. Oddershede, "Present state of the calculation of radiative lifetimes of molecules," *Physica Scripta*, vol. 20, no. 5-6, p. 587, 1979.

[34] E. Anderson, Z. Bai, C. Bischof, S. Blackford, J. Demmel, J. Dongarra, J. Du Croz, A. Greenbaum, S. Hammarling, A. McKenney, and D. Sorensen, *LAPACK Users' Guide*. Philadelphia, PA: Society for Industrial and Applied Mathematics, third ed., 1999.

[35] OpenMP Architecture Review Board, "OpenMP application program interface version 4.5," May 2015.

[36] L. Wolniewicz, "Variational treatment of the heh+ ion and the β-decay in ht," *The Journal of Chemical Physics*, vol. 43, no. 4, pp. 1087–1091, 1965.

[37] W. Kołos and J. Peek, "New ab initio potential curve and quasibound states of heh+," *Chemical Physics*, vol. 12, no. 4, pp. 381–386, 1976.

[38] D. M. Bishop and L. M. Cheung, "A theoretical investigation of heh+," *Journal of Molecular Spectroscopy*, vol. 75, no. 3, pp. 462–473, 1979.

[39] E. A. Engel, N. Doss, G. J. Harris, and J. Tennyson, "Calculated spectra for heh+ and its effect on the opacity of cool metal-poor stars," *Monthly Notices of the Royal Astronomical Society*, vol. 357, no. 2, pp. 471–477, 2005.

[40] J. A. Coxon and P. G. Hajigeorgiou, "Experimental born–oppenheimer potential for thex1σ+ ground state of heh+: Comparison with the ab initiopotential," *Journal of molecular spectroscopy*, vol. 193, no. 2, pp. 306–318, 1999.

[41] M. Stanke, D. Kedziera, M. Molski, S. Bubin, M. Barysz, and L. Adamowicz, "Convergence of experiment and theory on the pure vibrational spectrum of heh+," *Physical review letters*, vol. 96, no. 23, p. 233002, 2006.

[42] R. J. Le Roy and R. B. Bernstein, "Shape resonances and rotationally predissociating levels: The atomic collision time-delay functions and quasibound level properties of h 2 (x 1 σ g+)," *The Journal of Chemical Physics*, vol. 54, no. 12, pp. 5114–5126, 1971.

[43] C. J. Joachain, *Quantum collision theory*. Elsevier, 1975.

[44] W.-C. Tung, M. Pavanello, and L. Adamowicz, "Accurate potential energy curves for heh+ isotopologues," *The Journal of Chemical Physics*, vol. 137, no. 16, p. 164305, 2012.

Appendices

A Discrete Variable Representation (DVR)

To generate the Hamiltonian matrix, first, we calculate the kinetic energy contribution as follow:

$$T_{ii'} = \frac{\hbar^2(-1)^{i-i'}}{2m\Delta x}, \tag{16}$$

where Δx is the spacing between two points in the grid, and the equation is multiplied by

$$\frac{\pi^2}{3}, \qquad if \quad i = i'$$

or,

$$\frac{2}{(i-i')^2}, \qquad when \quad i \neq i'.$$

The potential energy is obtained by the diagonal form

$$V_{ii'} = \delta_{ii'} V(X_i) \tag{17}$$

and the grid points (x_i) are uniformly spaced

$$x_i = i\Delta x, \qquad i = 1,2,3,...$$

Finally, the matrix is conformed by the sum of the kinetic and potential energies.

B Sympletic Propagator

Eq. 8 can be written in the classical Hamilton form

$$\frac{dq(r)}{dr} = \frac{\partial h(p,q,r)}{\partial p}, \qquad \frac{dp(r)}{dr} = -\frac{\partial h(p,q,r)}{\partial p}, \tag{18}$$

where

$$q(r) = \psi(r), \qquad p(r) = \frac{d\psi(r)}{dr} \tag{19}$$

and

$$h(p,q,r) = \frac{1}{2}\left[p(r)^2 - w(r)q(r)^2\right], \tag{20}$$

with

$$w(r) = \frac{2\mu}{\hbar^2}\left[v(r) - E\right]. \tag{21}$$

Thus, the algorithm to evolve the positions and values of the wave function is presented as follow:

$$\begin{aligned} P_k &= P_{K-1} + b_k W(r_{k-1}) Q_{k-1} dr \\ Q_k &= Q_{k-1} + a_k P_k dr \\ r_k &= r_{k-1} + a_k dr \end{aligned} \tag{22}$$

C Rate Coefficients

Table 3: Rate constants for He + $H^+ \rightarrow HeH^+(X^1\Sigma^+)$

T(K)	$\alpha(T)^a$	$\alpha(T)^b$	$\alpha(T)^c$
1	0.77392800	0.78235481	0.78203179
10	2.5707441	2.61741437	2.60128530
20	2.08019694	2.11844464	2.10498152
30	1.62866434	1.65866504	1.64810387
40	1.36895183	1.39433715	1.38543034
50	1.21674617	1.23962475	1.23163666
70	1.07042766	1.09176926	1.08413254
100	0.99808402	1.02172366	1.01160630
200	0.92797193	0.96599119	0.94254824
300	0.85484479	0.89836279	0.87049235
400	0.78088387	0.82402242	0.79678959
500	0.71444877	0.75510830	0.73005339
1000	0.49396040	0.52127514	0.50627779
2000	0.30008319	0.31501765	0.30784400
3000	0.21027058	0.22009534	0.21569585
5000	0.12523387	0.13069340	0.12842585
10000	0.05544719	0.05769992	0.056834155
20000	0.022312913	0.23196821	0.022863178

[a] Obtained using the potential from the reference [24]
[b] Obtained using the potential from the reference [8]
[c] Present work

Table 4: Rate constants for $He^+ + H \rightarrow HeH^+(X^1\Sigma^+)$

T(K)	$\alpha(T)^a$	$\alpha(T)^b$	$\alpha(T)^c$
1	1.86326646	1.84386409	1.86337289
10	1.68376913	1.66581802	1.67976459
20	1.26992473	1.25596974	1.26577823
30	1.06977578	1.05792535	1.06580758
40	0.94547096	0.93493447	0.94164717
50	0.85853476	0.84892804	0.85483146
70	0.74184192	0.73354601	0.73836531
100	0.63533938	0.62837185	0.63218603
200	0.47281816	0.46828070	0.47043677
300	0.40147129	0.39811791	0.39942545
400	0.35987736	0.35746506	0.35821833
500	0.33227110	0.33045700	0.33081267
1000	0.26767200	0.26731909	0.26673702
2000	0.22873052	0.22903944	0.22816679
3000	0.21659441	0.21698511	0.21618196
5000	0.21282108	0.21318447	0.21255141
10000	0.22937230	0.22967158	0.22925400
20000	0.27020987	0.27048235	0.27022411

[a] Obtained using the potential from the reference [24]
[b] Obtained using the potential from the reference [8]
[c] Present work

Table 5: Rate constants for $He^+ + H \rightarrow HeH^+(A^1\Sigma^+)$

T(K)	$\alpha(T)^a$
1	1.95553346
10	1.80617656
20	1.52840151
30	1.36124399
40	1.22537527
50	1.11298741
70	0.94123362
100	0.76721468
200	0.47620469
300	0.34021514
400	0.26020897
500	0.20792211
1000	0.0949755
2000	0.0390600
3000	0.0224590
5000	0.0109249
10000	0.0040016
20000	0.0014407